

# Impact of Parallel-Threaded Mechanical Coupler Splices on the Seismic Behaviour of Reinforced Concrete Shear Walls

Nasser Mohamed<sup>1</sup>, Ferrier Emmanuel<sup>1</sup>, Michel Laurent<sup>1</sup>, Gabor Aron<sup>1</sup>, Huet Philippe<sup>2</sup>, Dolo Jean-Marie<sup>3</sup>

<sup>1</sup> Laboratoire LMC2, University Claude Bernard Lyon 1, 82 bd Niels Bohr, 69100 Villeurbanne, France

<sup>2</sup> LINXION The original of BARTEC, 355 Avenue Henri Schneider 69330 Meyzieu, France

<sup>3</sup> Eiffage Infrastructures, 3-7 place de l'Europe, Vélizy-Villacoublay, France

## Summary

This study assesses the performance of reinforced concrete (RC) shear walls utilizing mechanical couplers in comparison to traditional overlapping splices under both axial and cyclic loading conditions. Employing larger diameter splicing methods is critical for ensuring structural integrity in large constructions, where safety is paramount. Overlapping splices can result in congestion and poor construction quality due to the intricate detailing required in the joints. Conversely, mechanical couplers provide efficient installation and economic benefits. Three RC shear walls with various splicing configurations were tested under quasi-static cyclic lateral loading. The results demonstrated that mechanical couplers can improve ductility, energy dissipation, and stiffness. These findings suggest that mechanical couplers are a better alternative to traditional rebar overlapping splicing methods, to improve the overall performance of RC structures in large-scale construction projects as nuclear facilities.

## 1. Introduction

Rebar splicing in reinforced concrete (RC) structures is crucial for ensuring structural integrity, particularly in large-scale constructions like skyscrapers and industrial facilities. Commonly, the lap splice method, which connects rebars by overlapping them, is used. However, this method presents challenges when large rebars (greater than 16 mm in diameter) are involved. Codes such as Eurocode 2 [1], UBC 97 [2], and ACI 318-19 [3] provide guidelines for lap splicing. Eurocode 2 specifies that lap splices should not be placed in high-moment areas and must be symmetrically arranged. Where the lap length factors are influenced by the rebar's position, concrete strength, and rebar diameter. with a lap length calculated as:

$$l_d = \alpha_1 \alpha_2 \alpha_3 \alpha_5 \alpha_6 l_{b,req} \left( l_{b,req} = \left( \frac{d_b}{4} \right) \left( \frac{\sigma_{sd}}{f_{bd}} \right) \right) \geq l_{0,min} ; \text{ where } f_{bd} = 2.25 \eta_1 \eta_2 f_{cta} \quad (1)$$

where  $d_b$ : is the bar diameter  $\sigma_{sd}$ : is the design stress, and  $f_{bd}$ : is the bond strength, and  $f_{cta}$ : is the concrete tensile strength.

The lap splice method has limitations, particularly in large structures where rebar congestion, concrete honeycombing, and stress concentration are concerns. These issues impede concrete placement and can create air bubbles, leading to poor performance under static and dynamic loads [4], [5], [6], [7]. Lap splicing is simple to implement but often requires long rebar lengths, increasing both material and labor costs. The additional dead load from overlapping rebars (about 20%) also negatively impacts the structure.

Mechanical couplers offer a more efficient solution, improving ease of installation and reducing rebar usage. Couplers transfer stress directly between rebars, bypassing concrete interaction. Threaded couplers, the focus of this study, are particularly useful, as they allow the connection of rebars without requiring lap splices. International standards, such as ISO[8], dictate that slippage between the coupler and rebar must not exceed 0.10 mm.

Studies have demonstrated that mechanical couplers can meet or exceed the performance of lap splicing. Bompa and Elghazouli [9], [10] showed that threaded couplers improve ductility and energy dissipation in cyclic and monotonic tests. Dabiri and Kheyroddin [11] also confirmed that mechanical couplers perform well in terms of stiffness and elastic behavior when compared to continuous rebars. Bendahou et al. [12] carried out pull-out tests and bending tests on concrete beams which used compact mechanical couplers to connect rebar, and the results showed that the failure mode was the same as ordinary beams

In this study, four key aspects were investigated: (i) the bond strength between rebars connected using overlapping versus mechanical couplers, (ii) the mechanical influence of a new olive-shaped threaded coupler from LINXION The original of BARTEC, (iii) the effect of coupler positioning within columns, and (iv) the installation of double couplers spaced 320 mm apart on the same rebar. Cyclic load tests were performed to evaluate the performance of the couplers in column-to-foundation connections. The results indicated that mechanical couplers significantly improved the mechanical behavior compared to lap splices. The failure modes, crack openings in the plastic hinge zone, and nonlinear behavior of columns were analyzed and validated using the flexure-controlled ultimate and yielding chord rotation models defined in Eurocode 8[13].

## 2. Experimental setup

The primary aim of this study was to assess the impact of using mechanically spliced bars in reinforced concrete (RC) shear walls subjected to axial and cyclic loading. Three RC shear walls were constructed and tested. The experimental specimens consisted of two main parts: the foundation and the shear wall. The width, height, and length of the shear walls were 200 mm, 600 mm, and 2100 mm, respectively. The foundation was deliberately over-reinforced with a meshing of  $\text{Ø}16@85$  mm, adhering to Eurocode 8 seismic provisions with dimensions of  $1800 \text{ mm} \times 1100 \text{ mm} \times 600 \text{ mm}$ ., to prevent foundation failure and focus on the behavior of the connection between the shear wall and foundation. The study's design ensured that failure would occur within the shear wall and not the foundation. A lateral load was applied 1900 mm from the bottom of the shear wall using a setup fixed on both sides of the wall, as shown in Figure 1(left). The lateral load was determined based on the control displacement protocol, as shown in Figure 2(right).

The loading history followed was the same as in [14], [15], [16], where sinusoidal displacement-controlled loading was applied at 100 mm/min until the post-peak strength dropped to 85% or significant damage occurred. For the axial load, a self-compression technique was employed, with a hydraulic jack fixed on top of the shear wall, secured by a steel beam and 32-mm rebars connected to the foundation. A steel plate was installed at the top to ensure even distribution of the applied axial force across the shear wall. The axial load applied was  $n = 0.1 \times f'c \times A_g$ . The experimental setup was designed with a safety factor of three. The experimental details are depicted in Figure 1(left). The setup was connected to a displacement control machine capable of pushing and pulling, anchored to the diaphragm wall to ensure stability.

The shear walls were reinforced with ten 16-mm diameter rebars for longitudinal reinforcement and 10-mm diameter rebars as stirrups for transverse reinforcement. The concrete and rebar properties remained the same in all configurations. To evaluate concrete strength, 18 cylindrical specimens ( $\text{Ø}16 \times 32$  cm) were tested for compressive strength, and 6 specimens were subjected to tensile tests for splitting tensile strength. These samples were tested on the day of the experiment, ensuring 28 days had passed since casting. The average compressive strength and splitting tensile strength were 37 MPa and 3.2 MPa, respectively.

The B500B ribbed threaded steel rebars were threaded using a Linxion (Bartec) machine, with redesigned olive-shaped couplers that are thinner than typical cylindrical ones, as shown in Figure 2(left). Two splicing techniques were used: overlapping splicing and mechanical coupler batching. For the overlapping reference (OLR) specimens, two mechanical couplers were spaced 320 mm apart. The coupler connections were placed at varying heights (CSL) couplers at the same level and (CDL) couplers at different level, as illustrated in Figure 1(right). To ensure effective lateral load transfer to the top of the shear wall, a high-resistance steel plate was designed and fixed at 1900 mm from the base of the wall. This steel plate was connected to the lateral load machine and treated as a pin connection to restrain both vertical and horizontal degrees of freedom. The connection between the load cell and frame was designed as a roller, allowing movement under lateral loads.

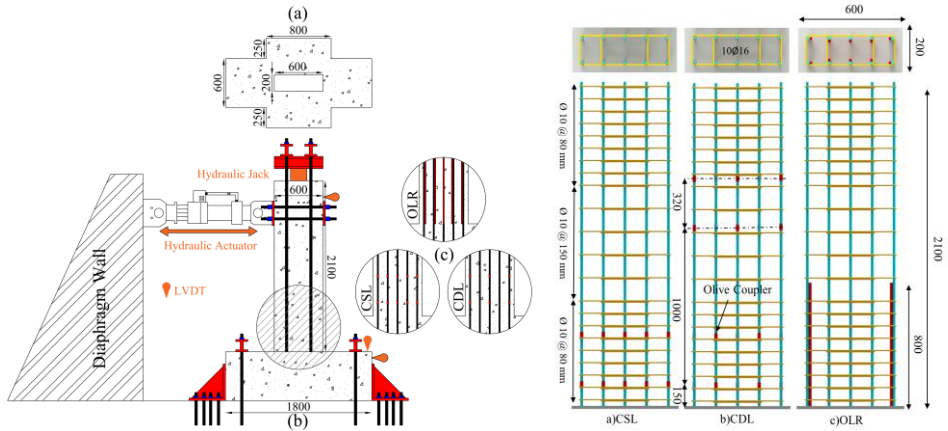


Figure 1: (Left) Schematic representation of: (a) foundation, (b) shear-wall experimental setup, and (c) connection method. (Right) Reinforced concrete (RC) detailing for the three specimens, showing both top and side views. The red-highlighted sections indicate the olive-shaped coupler, while the arrow labeled "800 mm" represents the overlap length extending from the foundation.

As shown in Figure 1(left), three linear variable differential transformer (LVDT) sensors were installed at critical points: one at the top of the shear wall, at 1900 mm from the base, and two on the foundation to measure its horizontal and vertical movements. These sensors ensured accurate data collection through corrections in the experimental results. Three key parameters from [17] were incorporated to promote flexural failure and optimize the design:  $2 \leq \lambda = H_0/D \leq 6$ ,  $1\% \leq \rho_v \leq 3\%$ , and  $n \leq 0.2$ , where  $\lambda$  is the shear aspect ratio,  $\rho_v$  is the volume of transverse reinforcement,  $H_0$  is the effective height of the shear wall,  $D$  is the column depth, and  $n$  is the axial load ratio. These parameters were crucial for ensuring flexural failure in the RC shear walls, facilitating a clear and accurate analysis of the experimental results.

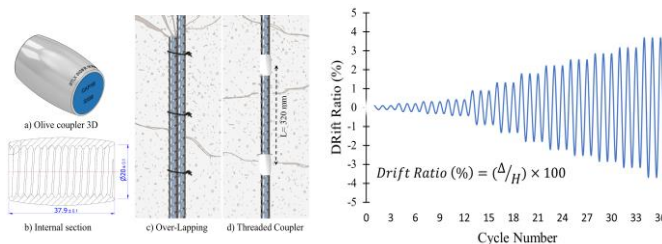


Figure 2 : (Left) Geometry of the olive-shaped coupler and splicing technique used for integrating shear walls with foundations. (Right) Loading protocol following ASTM E2126.

### 3. Hysteresis Curve and Eurocode Verification of Chord Rotation

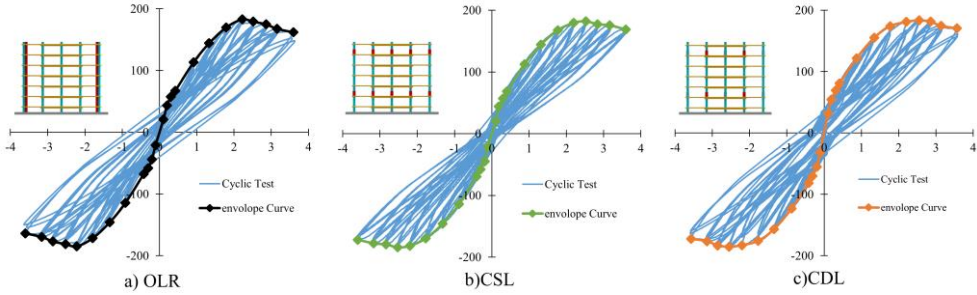


Figure 3: Force–displacement hysteresis curves for the three specimens.

The Figure 3 below illustrates the hysteresis curves, with the envelope curves extracted by taking the maximum values at each loading cycle. These envelope curves are critical for deriving the chord rotation, which measures the displacement capacity of structural elements, and for calculating the ductility, reflecting the structural behavior under seismic loads. While the global behavior of the different specimens appears generally similar, a detailed evaluation of stiffness, energy dissipation, and ductility is necessary to demonstrate their distinct performance under cyclic loading conditions. These assessments provide a deeper understanding of their seismic performance. The following section transitions into Eurocode 8 (EN 1998-3)[13] validation, where chord rotation parameters, including yielding and ultimate curvatures, are assessed. These parameters are crucial for evaluating the seismic performance of the shear-wall, ensuring that the experimental results align with Eurocode standards. To provide a concise overview of the key findings, the table below summarizes the main points for each specimen, including the yielding point, ultimate load, peak load, drift ratio, and theoretical ultimate values. A comparison between theoretical and experimental results is also presented.

Key points	Yielding point		Peak point		Ultimate point		Drift Ratio			
Specimen	$\Delta_y$ (mm)	$V_y$ (kN)	$\Delta_p$ (mm)	$V_p$ (kN)	$\Delta_u$ (mm)	$V_u$ (kN)	$\theta_{y(exp)}$	$\theta_{y(the)}$	$\theta_{u(exp)}$	$\theta_{u(the)}$ /yel
OLR	31.3	161.92	42.22	182.8	76	155	1.64	1.75	4	3.8
CSL	30.6	159.5	47.9	182	85	154	1.61	1.75	4.4	4.2
CDL	27.77	160.5	48.5	183.75	90	156	1.49	1.75	4.7	4.2

Table 1 : Key points extracted from the hysteresis curves, including the yielding point (onset of yielding), peak point (maximum lateral load capacity), and ultimate point (15% reduction from peak load). Both theoretical and experimental values for elastic and ultimate deformations (drift) are provided for comparison, based on the formulas proposed by Biskinis and Fardis. [18].

The seismic design principles outlined in Eurocode 8 (EN 1998-3) [13] emphasize displacement capacity as a key measure of structural performance during seismic events. This capacity is expressed through chord rotation, calculated using the yielding curvature ( $\varphi_y$ ) and ultimate curvature ( $\varphi_u$ ). For elastic chord rotation ( $\theta_y$ ), For shear walls with continuous longitudinal bars in the plastic hinge region, the ultimate chord rotation ( $\theta_u$ ), and for columns with lap-spliced bars, the ultimate chord rotation is defined by equation 7-8-9 respectively:

$$\theta_{y(the)} = \varphi_y \frac{L_s + \alpha_{vz}}{3} + 0.0013 \left( 1 + 1.5 \frac{h}{L_s} \right) + \alpha_{st} \theta_{y,stip} \quad (2)$$

$$\theta_{u(the)} = \alpha_{st} (1 - 0.43 \alpha_{cy}) \left( 1 - \frac{3}{8} \alpha_{w,r} \right) \left( 1 + \frac{\alpha_{sl}}{2} \right) (0.3)^{\nu} \left( \frac{\max(0.01, w_2)}{\max(0.01, w_1)} f_c \right)^{0.225} \left( \frac{L_s}{h} \right)^{0.35} 25^{\left( \frac{\alpha_{\rho_s} f_{yw}}{f_c} \right)} (1.25)^{100 \rho d} \quad (3)$$

$$\theta_{u(the)} = \left( \frac{l_o}{l_{o,min}} \right) [\theta_{u(Eqs. 3.3b)}] \text{ if } l_o < (l_{o,min} = d_{bl} f_{yl} [(1.05 + 14.5 \alpha_1 \rho_s f_{yw} / f_c) \sqrt{f_c}]) \quad (4)$$

Both theoretical and experimental values of  $\theta_u$  align well, validating the accuracy of the test results. When applying a safety factor ( $\gamma_{el} = 1.5$ ), the recalculated displacement leads to a force reduction to

85%-80% of the maximum force . This Eurocode validation confirms the reliability of the experimental test in simulating real-world seismic behavior compared to the experimentale tests already done.

#### 4. Crack Opening observation by digital image corelation

We can observe several key findings from the failure mode of the shear wall in Figure 4(left). First, the crack accumulation is notably less in the OLR (overlapping rebar) specimens compared to those with couplers (CSL and CDL). Specifically, in the region between 0 to 500 mm, which is considered the plastic hinge zone of the columns, the number of cracks in the OLR specimens is lower. The total top displacement is influenced by two primary factors: crack development along the column height and the edge uplifting of the column as shown in Figure 4(right)(a). Using Digital Image Correlation (DIC), we were able to quantify the crack distribution within the plastic hinge zone, we observed that the CSL and CDL specimens exhibit similar behavior, while the OLR specimens show fewer cracks Figure 4(right)(c). Additionally, by identifying the edge uplifting of the column Figure 4(right)(b), we found that the OLR specimens experience a more significant and sharper increase in uplifting, indicating that stress concentration is accumulating near the base of the column where the overlapping begins. In conclusion, our observations suggest that the use of couplers, compared to overlapping rebars (OLR), results in a more uniform stress distribution, which leads to less catastrophic failures. This is reflected in the reduced edge uplifting and more controlled failure mode in the specimens with couplers.

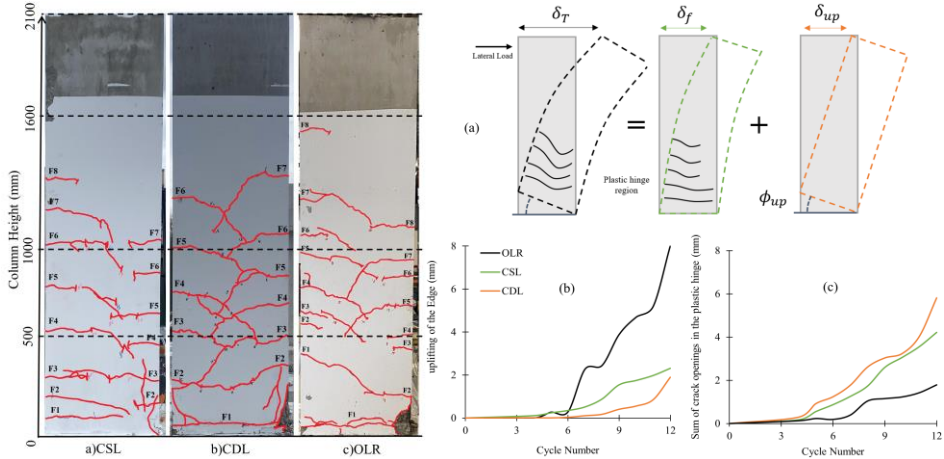


Figure 4: (Left) Shear wall failure mode. (Right) (a) Total displacement demonstration, (b) Edge uplifting of the shear wall, and (c) Sum of crack openings in the plastic hinge zone of the shear wall.

#### 5. Discussion

##### a) Ductility of Shear Walls

Ductility is calculated using the equation:

$$\mu = \frac{\Delta_u}{\Delta_y} \quad (5)$$

Where  $\Delta_u$  represents the displacement at a 15% decrease in  $F_{max}$ , indicating significant load reduction post-peak [19], and  $\Delta_y$  is determined using the secant stiffness method. This method accounts for stiffness reduction due to cracking, with the yield displacement determined by intersecting the hysteresis curve at  $0.75V_{peak}$  Figure 5(left). Key points from the hysteresis curves, including the yielding, ultimate, and peak points, are summarized in Table 1. Figure 5(right) shows ductility values, with comparisons to a reference shear wall OLR. The specimen with overlap splices (OLR) exhibits the lowest ductility. Among shear walls with parallel-threaded couplers, CSL shows a 14% increase in ductility compared to the reference, while CDL has the highest improvement at 33%. This demonstrates that the placement of threaded couplers significantly influences shear wall ductility. Specifically, placing all

threaded couplers at the bottom of the shear wall results in a slight ductility enhancement compared to OLR, while positioning half of the couplers 1000 mm above the bottom increases ductility by 33%. So OLR has the lowest  $\Delta u$ . All specimens with mechanical coupler connection show increased ultimate displacement, with configurations placing half the couplers at the bottom yielding the highest  $\Delta u$  as shown in Table 1 : Key points extracted from the hysteresis curves, including the yielding point (onset of yielding), peak point (maximum lateral load capacity), and ultimate point (15% reduction from peak load). Both theoretical and experimental values for elastic and ultimate deformations (drift) are provided for comparison, based on the formulas proposed by Biskinis and Fardis. [18] ..

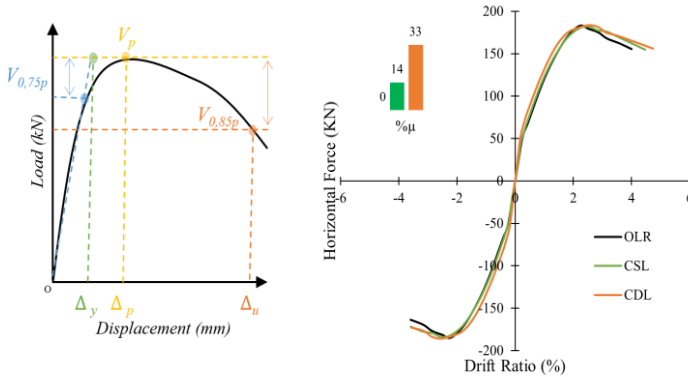


Figure 5: (Left) Method used to determine key displacement values:  $\Delta y$  (yielding displacement),  $\Delta u$  (ultimate displacement),  $\Delta_{0.85p}$  (displacement at 15% peak load reduction),  $\Delta_{0.75p}$  (displacement at 25% peak load), and  $\Delta p$  (peak displacement). (Right) Force-drift ratio envelope curves for the specimens.

b) The dissipated energy (DE)

ED is measured by the area enclosed within the hysteresis loop for each load cycle Figure 6 [19], [20], and cumulative dissipated energy (CDE) is calculated by summing the DE from previous cycles. Initially, up to a 1.5% drift ratio, all shear-walls performed similarly with low CDE values, indicating minimal impact of different bar splices on cyclic behavior under low loads. From 1.5% to 3.5% drift, CDE increased significantly in all specimens, with the CDL specimen the highest CDE beyond a 3.5% drift ratio. Conversely, OLR exhibited the lowest CDE, while CSL showed slightly higher CDE compared to the OLR.

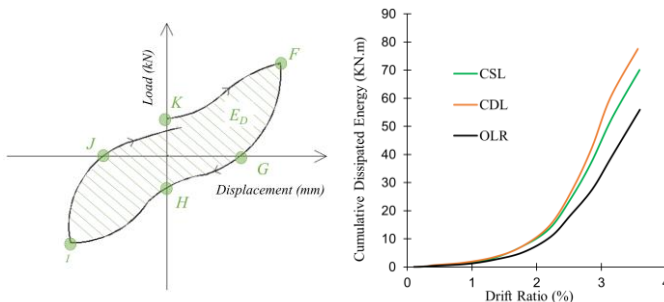


Figure 6: (Left) Method used to determine ED (energy dissipated). (Right) Cumulative dissipated energy of the specimens.

c) Secant Stiffness

As shown in Figure 7(left), the stiffness under cyclic loading is calculated using the equation:

$$K_s = \frac{|F_j^+| + |F_j^-|}{|\delta_j^+| + |\delta_j^-|} \quad (6)$$

where  $F_j^+$  and  $F_j^-$  are the maximum loads in the forward and reverse directions of the  $j^{\text{th}}$  loading level, respectively, and  $\delta_j^+$  and  $\delta_j^-$  are the maximum displacements in the forward and reverse directions of the  $j^{\text{th}}$  loading level, respectively. The stiffness degradation coefficient is defined as the ratio of the secant stiffness to the initial stiffness, as illustrated in Figure 7(left) [21]. Initially, as shown in Figure 7(right) CSL and CDL showed enhanced stiffness to OLR, OLR had a considered reduction. Before a 1.5% drift ratio, overlapping splices exhibited greater stiffness degradation, but all specimens demonstrated consistent behavior after the 1.5% drift. This analysis highlights the differential impacts of the splice type and configuration on the stiffness degradation behaviour of RC shearwall under cyclic loading.

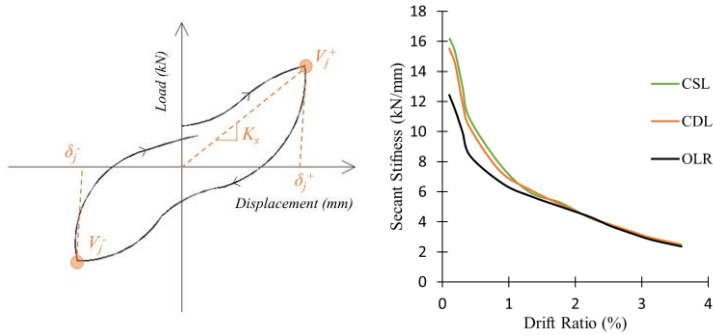


Figure 7 : (Left) Method used to determine  $K_s$  (Secant Stiffness)  $\delta_j^+$  (positive drift displacement),  $V_j^+$  (positive shear load),  $\delta_j^-$  (negative drift displacement), and  $V_j^-$  (negative shear load). (Right) Stiffness curves for all specimens.

## 6. Summary and Conclusions

This study focused on the performance of reinforced concrete (RC) shear walls with mechanical couplers compared to traditional overlapping splices under axial and cyclic loading. In large-scale RC constructions, splicing is crucial for maintaining structural integrity, especially when using large-diameter rebars. While overlapping splices are widely used, they can create issues such as rebar congestion, reduced construction quality, and complications in achieving proper concrete pouring, particularly in critical joint regions. Mechanical couplers, in contrast, offer advantages in terms of easier installation, economic efficiency, and improved structural performance.

Three RC shear walls with different splicing configurations were subjected to quasi-static cyclic lateral loading to assess key parameters such as ductility, stiffness, and energy dissipation. The experimental tests provided detailed insight into the behavior of shear walls with mechanical couplers under loading, revealing that these couplers significantly enhance structural performance.

1. **Ductility and Energy Dissipation:** Shear walls incorporating mechanical couplers demonstrated higher ductility and energy dissipation compared to those with traditional overlapping splices. These couplers improved the overall seismic resilience of the structures, especially at higher drift ratios.
2. **Stiffness:** The stiffness degradation of shear walls with mechanical couplers was better than the overlapping rebars, maintaining stability throughout the cyclic loading. Walls with overlapping splices showed greater stiffness reduction, particularly beyond the 2% drift ratio.
3. **Eurocode Verification:** The use of mechanical couplers complies with Eurocode standards, confirming their ability to meet seismic design requirements, including displacement capacity and ultimate deflection.

In conclusion, mechanical couplers in RC shear walls significantly enhance ductility, stiffness retention, and energy dissipation, making them a superior alternative to traditional overlapping splices. These findings support the use of mechanical couplers for improved structural performance and compliance with Eurocode seismic design standards.

## 7. References

- [1] Eurocode 2, *Design of Concrete Structures, Part 1–1: General Rules for Buildings*. CEN, Brussels (Belgium), 2004.
- [2] I. C. of B. Officials, *Uniform Building Code*. International Council of Building Officials, 1997.
- [3] ACI Committee 318, *Building code requirement for structural concrete and commentary*. American Concrete Institute, 2019.
- [4] H. Dabiri, A. Kheyroddin, and A. Dall’Asta, “Splice methods used for reinforcement steel bars: A state-of-the-art review,” *Constr. Build. Mater.*, vol. 320, p. 126198, 2022, doi: <https://doi.org/10.1016/j.conbuildmat.2021.126198>.
- [5] G. Metelli, J. Cairns, and G. Plizzari, “The influence of percentage of bars lapped on performance of splices,” *Mater. Struct.*, vol. 48, pp. 2983–2996, Sep. 2015, doi: 10.1617/s11527-014-0371-y.
- [6] R. Mabrouk and A. Mounir, “Behavior of RC beams with tension lap splices confined with transverse reinforcement using different types of concrete under pure bending,” *Alex. Eng. J.*, vol. 57, Jun. 2017, doi: 10.1016/j.aej.2017.05.001.
- [7] R. Alyousef, T. Topper, and A. Al-Mayah, “Crack growth modeling of tension lap spliced reinforced concrete beams strengthened with fibre reinforced polymer wrapping under fatigue loading,” *Constr. Build. Mater.*, vol. 166, pp. 345–355, 2018, doi: 10.1016/j.conbuildmat.2018.01.136.
- [8] *Steels for the reinforcement of concrete — Reinforcement couplers for mechanical splices of bars — Part 1: Requirements*, First edition. Geneva, Switzerland: International Organization for Standardization, 2009.
- [9] D. Bompa and A. Elghazouli, “Monotonic and cyclic performance of threaded reinforcement splices,” in *Structures*, Elsevier, 2018, pp. 358–372.
- [10] D. Bompa and A. Y. Elghazouli, “Inelastic cyclic behaviour of RC members incorporating threaded reinforcement couplers,” *Eng. Struct.*, vol. 180, pp. 468–483, Feb. 2019, doi: 10.1016/j.engstruct.2018.11.053.
- [11] A. Kheyroddin, A. Mohammadkhal, H. Dabiri, and A. Kaviani, “Experimental investigation of using mechanical splices on the cyclic performance of RC columns,” in *Structures*, Elsevier, 2020, pp. 717–727.
- [12] A. Ben-dahou *et al.*, “Influence of rebar couplers on the cracking behavior of reinforced concrete beams,” *Nucl. Eng. Des.*, vol. 416, p. 112801, Jan. 2024, doi: 10.1016/j.nucengdes.2023.112801.
- [13] E. C. for Standardization, *Eurocode 8: Design of Structures for Earthquake Resistance*. CEN, 2004.
- [14] F. Di Luccio *et al.*, “Seismic signature of active intrusions in mountain chains,” *Sci. Adv.*, vol. 4, p. e1701825, Jan. 2018, doi: 10.1126/sciadv.1701825.
- [15] N. Reboul, Z. Mesticou, A. Si Larbi, and E. Ferrier, “Experimental study of the in-plane cyclic behaviour of masonry walls strengthened by composite materials,” *Constr. Build. Mater.*, vol. 194, pp. 70–83, Mar. 2018, doi: 10.1016/j.conbuildmat.2017.12.215.
- [16] S. Qazi, L. Michel, and E. Ferrier, “Seismic behaviour of RC short shear wall strengthened with externally bonded CFRP strips,” *Compos. Struct.*, vol. 211, pp. 390–400, 2019, doi: <https://doi.org/10.1016/j.compstruct.2018.12.038>.
- [17] M. Ying and J. Gong, “Seismic Failure Modes and Deformation Capacity of Reinforced Concrete Columns under Cyclic Loads,” *Period. Polytech. Civ. Eng.*, vol. 62, Jun. 2017, doi: 10.3311/PPci.9893.
- [18] D. E. Biskinis and M. N. Fardis, “Cyclic Deformation Capacity, Resistance and Effective Stiffness of RC Members with or without Retrofitting,” in *Proceedings of the 14th World Conference on Earthquake Engineering*, Patras, Greece: Structures Lab, Dept. of Civil Engineering, University of Patras, October 12–17.
- [19] R. Park, “State of art report ductility evaluation from laboratory and analytical testing,” in *Proceedings of the 9th World Conference on Earthquake Engineering*, 1988, p. 605.
- [20] China Academy of Building Research, *Specification for seismic test of buildings*. China Academy of Building Research, 2015.
- [21] F. E. M. Agency, “Interim Protocols for Determining Seismic Performance Characteristics of Structural and Nonstructural Components through Laboratory Testing,” Federal Emergency Management Agency, Redwood City, CA, USA, FEMA-461, 2007.

